PCCP

PAPER

View Article Online
View Journal | View Issue

Cite this: *Phys. Chem. Chem. Phys.*, 2019, **21**, 15040

Ultrafast decay dynamics of water molecules excited to electronic $\tilde{D}'$ and $\tilde{D}''$ states: a time-resolved photoelectron spectroscopy study

Yanjun Min,†[ab] Dongyuan Yang,†[ab] Zhigang He,[a] Zhichao Chen,[a] Kaijun Yuan,[a] Dongxu Dai,[a] Guorong Wu *[a] and Xueming Yang[a]

Received 24th March 2019,
Accepted 14th June 2019

DOI: 10.1039/c9cp01644a

rsc.li/pccp

The ultrafast decay dynamics of water molecules excited to $\tilde{D}'^1B_1$ and $\tilde{D}''^1A_2$ states is studied by combining two-photon excitation and time-resolved photoelectron imaging methods. The lifetime of the $\tilde{D}'^1B_1(000)$ state of H_2O (D_2O) is determined to be 1.54 ± 0.1 (22.6 ± 1.6) ps, consistent with a previous high-resolution spectroscopic study. The H_2O $\tilde{D}''^1A_2(000)$ state decays with a lifetime of 4.1 ± 0.2 ps, while in the D_2O $\tilde{D}''^1A_2(000)$ state, two independent decay pathways are observed, with time constants of 0.55 ± 0.1 and 13 ± 1 ps, respectively. The former is proposed to be associated with a hitherto undocumented $\tilde{D}'' \rightarrow \tilde{C}$ pathway, induced by Coriolis interaction.

Introduction

Photochemistry of water in the gas phase is one of the most important, yet challenging topics in molecular reaction dynamics. It has served as an ideal model system for the understanding of complicated photodissociation dynamics of polyatomic molecules. It is also of practical importance for the study of atmospheric and interstellar photochemistry. In the last four decades, numerous experimental and theoretical studies have been devoted to this system from which many details of the photochemical and photophysical processes of water molecules in electronically excited states have been revealed.[1–7]

Most of experimental studies so far are of frequency-domain, *i.e.*, energy resolved, due to the lack of wavelength tunable ultrafast VUV laser sources. In the last couple of years, we have studied the ultrafast decay dynamics of water molecules excited to $\tilde{C}^1B_1$, $\tilde{D}^1A_1$, $\tilde{F}^1B_1$ and $\tilde{F}^1A_1$ states, by combining two-photon absorption excitation and time-resolved photoelectron imaging (TRPEI) methods.[6,8] The detailed ultrafast decay dynamics of these states is studied. Along with the information from energy-resolved studies on these states,[5,9–11] the understanding of the photochemistry of water molecules excited to these states is improved. Following previous studies, we further study the ultrafast decay dynamics of another two high-lying electronic states: $\tilde{D}'^1B_1$ and $\tilde{D}''^1A_2$.

Both $\tilde{D}'^1B_1$ and $\tilde{D}''^1A_2$ states are of Rydberg character with an electron from the highest occupied molecular orbital (HOMO) excited to $4sa_1$ and $3db_2$, respectively. In a high-resolution spectroscopic study by Ashfold and coworkers, the predissociation rates and mechanisms of these two states were investigated by simulating the rotational intensity distribution in the 3 + 1 resonance-enhanced multi-photon ionization (REMPI) spectra.[12] The H_2O $\tilde{D}'(000)$ state predissociates with a lifetime of 1.3 ps (a natural linewidth of 4 cm^{-1}) to the $\tilde{A}^1B_1$ through homogeneous (rotational level independent) pure electronic coupling. [The vibronic state notation is such that $(n_1n_2n_3)$ designates the state with n_1, n_2 and n_3 quantum excitation in the ν_1, ν_2 and ν_3 vibrational modes, respectively.] For D_2O $\tilde{D}'(000)$, in addition to the homogeneous pathway, there is also a heterogeneous (rotational level dependent) predissociation pathway *via* Coriolis interaction with the $\tilde{D}^1A_1$ state induced by rotation about the molecular *a*-axis, resulting in a lifetime of 106 ps for the ground rotational state and a moderate decrease of lifetime with the increase of $\langle \hat{J}_a^2 \rangle$ (the expectation value of the square of the rotational angular momentum about the molecular *a*-axis). For the $\tilde{D}''(000)$ state, both homogeneous and heterogeneous mechanisms play roles. But the Coriolis interaction is induced by rotation around different molecular axes: *a*-axis for H_2O and *b*-axis for D_2O.

In this paper, we present a fs time-resolved study on the ultrafast decay dynamics of water molecules excited to the $\tilde{D}'^1B_1$ and $\tilde{D}''^1A_2$ states, by combining two-photon excitation and TRPEI methods. The lifetimes of these two states are measured and the decay dynamics is discussed. In Section II, we describe the experimental methods used. In Section III, the analysis of the experimental data and a brief discussion of the decay mechanisms of these two states are provided. In Section IV, short conclusions are provided.

[a] *State Key Laboratory of Molecular Reaction Dynamics, Dalian Institute of Chemical Physics, 457 Zhongshan Road, Dalian 116023, Liaoning, China. E-mail: wugr@dicp.ac.cn*
[b] *University of Chinese Academy of Sciences, Beijing 100049, China*
† These authors contributed equally.

Experimental

The methods and experimental apparatus have been described in previous publications;[6,8,13] therefore, only primary features are presented here. The $\tilde{D}'$ and $\tilde{D}''$ states were excited by two-photon absorption at ~236 and ~232 nm respectively, whereupon another delayed laser pulse probed the excited state *via* one-photon ionization. Both pump and probe laser pulses were obtained from a fully integrated Ti:Sapphire oscillator/regenerative amplifier system (<50 fs, 800 nm, 3.8 mJ and 1 kHz, Coherent, Libra-HE), followed by two optical parametric amplifiers (OPA, Coherent, OperA Solo), each pumped by a fraction (1.3 mJ) of the fundamental output of the amplifier. For the $\tilde{D}''$ state, the probe laser pulse (330.8 nm, ~4 μJ) was obtained directly from one of the OPAs. The bandwidth (full width at half maximum (FWHM) of the spectrum) of the 330.8 nm laser pulse was 413 cm^{-1}. For the pump laser (231.8 and 232.0 nm for the H_2O and D_2O, respectively), the output of the other OPA at ~551 nm (~20 μJ) was mixed with a 400 nm laser beam (~50 μJ) using a β-BBO crystal (0.15 mm), which was generated by doubling of a fraction of (~300 μJ) 800 nm using another β-BBO crystal (0.1 mm). The bandwidths of 231.8 and 232.0 nm are 198 and 188 cm^{-1}, respectively. For the $\tilde{D}'$ state, two different schemes were used to generate pump and probe pulses: (1) for H_2O, a laser beam at 400.0 nm (a bandwidth of 300 cm^{-1}, ~5 μJ), generated by doubling a fraction of 800 nm (~0.1 mJ) using a 0.1 mm β-BBO crystal, was used as the probe pulse. For the pump pulse, the output of one OPA at ~672 nm (~29 μJ) was doubled using a β-BBO (2 mm) which was further mixed with a fraction of 800 nm to generate 236.5 nm (a bandwidth of 178 cm^{-1}, ~1.8 μJ) using a 0.1 mm β-BBO crystal. (2) For D_2O, the pump laser beam (236.3 nm, 28 cm^{-1}, ~2.4 μJ) was generated by doubling the output of one of the OPAs at 472.6 nm. A β-BBO crystal of thickness (2 mm) much larger than that allowed by the group velocity mismatch was used to greatly reduce the bandwidth of 236.3 nm in order to enhance the two-photon absorption efficiency (*vide infra*). A much longer probe wavelength (478.1 nm, 240 cm^{-1}, 13 μJ) was also used to reduce some unintended multi-photon ionization signals.[8]

The pump and probe laser pulses were combined collinearly using a dichroic mirror without further compression, and then focused using an f/75 lens to intersect a seeded water molecular beam in the interaction region of the velocity map imaging (VMI) spectrometer. The water molecular beams were generated by bubbling He of ~4 bar through water samples at room temperature using an Even-Lavie pulsed valve operating at 1 kHz. Both the pump and probe pulses were linearly polarized with the polarization direction parallel to the micro channel plate/phosphor screen detector. Time delays between the pump and probe pulses were scanned using a motorized linear translation stage (Newport, M-ILS250HA) which was located upstream of one of the OPAs. The photoelectron images arising from the pump and probe lasers alone were also recorded. The sum of the single color photoelectron images was subtracted in order to correct for background photoelectrons generated from single color multi-photon ionizations. The 2D photoelectron image was transferred to the 3D distribution using the polar basis function expansion method.[14] The time-dependent photoelectron 3D distributions were further integrated along the recoiling angle to derive the kinetic energy distributions of the photoelectron, *i.e.*, time-resolved photoelectron spectra (TRPES).

Electron kinetic energy calibration was achieved using multi-photon ionization of a Xe atom. This also served to measure the cross-correlation (*i.e.*, instrumental response function, IRF) between the pump and probe laser pulses. For the analysis of the TRPES data for the $\tilde{D}''$ state, the time delay-dependent curves of the electron yield were fitted to a Gaussian function, based on the approximation that both pump and probe laser pulses have a Gaussian profile. This analysis provides not only the FWHM width of the IRF, but also the uncertainty of this width. As for the $\tilde{D}'$ state, the time delay-dependent curves of the electron yield were far from a Gaussian profile due to the very thick β-BBO used in the generation of pump laser pulses, and the curves were used directly in the TRPES data analysis. It has to be noted here that only photoelectrons generated by absorption of two pump photons and a single probe photon were taken into account in this analysis, thanks to the capability of the VMI technique in differentially analyzing the outgoing photoelectron as a function of delay with respect to kinetic energy. The time-zero overlap and molecular beam conditions were checked before and after the TRPES measurement to make sure there was no severe drift of the time-zero during measurement.

Results and discussion

Water molecules were excited into $\tilde{D}'$ or $\tilde{D}''$ states by two-photon absorption whereupon another delayed laser pulse probed the excited state water molecules *via* one-photon ionization (Fig. 1). In the following, we present the experimental results for these two states separately, each accompanied by a brief discussion on the ultrafast decay dynamics.

The $\tilde{D}'^1B_1$ state

Fig. 2(a) shows the TRPES data of H_2O at a pump wavelength of 236.5 nm. The TRPES data are mainly comprised of two features: a strong feature around time-zero spreading over all kinetic energies, showing a very fast decay dynamics, and two narrow peaks, located at 0.9–1.0 eV and 0.4–0.6 eV, showing a ps decay dynamics. The former is presumably associated with some undesired two-color multi-photon ionization processes, with no electronic state or electronic states of very short lifetimes as intermediate resonance. This feature was also found in previous studies of the ultrafast decay dynamics of the $\tilde{C}$ and $\tilde{F}$ states of water molecules for which the same experimental methods were used.[6,8] The origin of this feature is not considered in the current study and no further discussion is provided. The kinetic energies of the ps feature perfectly match the energetic limits for photo-ionization to $D_0(000)$ and (100) of H_2O^+.[12,15,16] The photoelectron kinetic energy distribution for the latter feature is better presented in Fig. 2(b) which is derived by integrating the TRPES data in Fig. 2(a) over the time delay range of 0.3–6 ps.

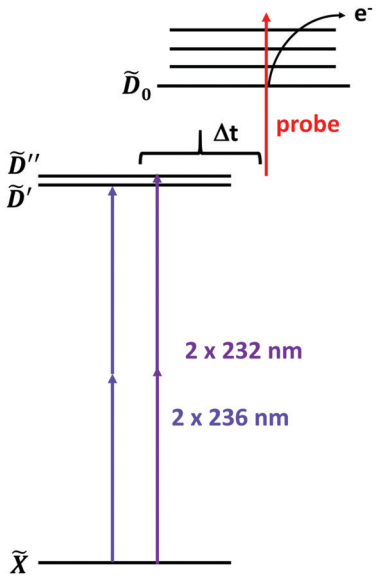

Fig. 1 Schematic presentation of the femtosecond pump–probe TRPEI study of water molecules excited to D̃′ and D̃″ states.

In Fig. 2(c), the photoelectron transient (the time delay dependence of the photoelectron signal), derived by integrating the TRPES data over photoelectron kinetic energy ranges of 0.4–0.6 eV and 0.85–1.05 eV, is shown. A least-squares method was employed to fit the photoelectron transient to extract the lifetime of the D̃′ state. The kinetic model used is expressed as follows:

$$S(t) = A_1\mathrm{IRF} + A_2\left[H(t)\exp\left(-\frac{t}{\tau}\right)\right] \otimes \mathrm{IRF} \qquad (1)$$

Here $S(t)$ represents the photoelectron transient and $H(t)$ the unit step function. The first part of the right side represents the contribution from the feature around time zero, and the other half, the convolution of $A_2[H(t)\exp(-t/\tau)]$ and IRF, the contribution from the D̃′ state. In the fit, time-zero was varied in the range of the experimentally measured time-zero drift to obtain the best fit. This analysis also served to estimate the confidence intervals of the lifetime constant. The lifetime of the D̃′ state was determined to be 1.54 ± 0.10 ps.

In the experiment with D_2O, there was no discernable signal associated with the D̃′ state observed when the pump laser pulse for that of H_2O was used. The D̃′ state lifetime of D_2O was determined to be much longer than that of H_2O and a much sharper and more discrete REMPI spectrum is expected.[12] In this regard, the two-photon absorption of the broad-bandwidth pump laser pulse is expected to be very inefficient. In the experiment, the bandwidth of the pump laser pulse was greatly reduced (from 120 to 23 cm^{-1}) by using a thick (2 mm) β-BBO crystal (see the Experimental section). With such a narrower bandwidth pump laser pulse, a very weak, but discernable feature associated with the D̃′ state was observed, as shown in Fig. 3(a). The tail towards negative delays is from the pump–probe cross-correlation profile and is due to the thick β-BBO crystal used. In Fig. 3(b), the photoelectron transient, derived by integrating the TRPES data over the kinetic energy range of

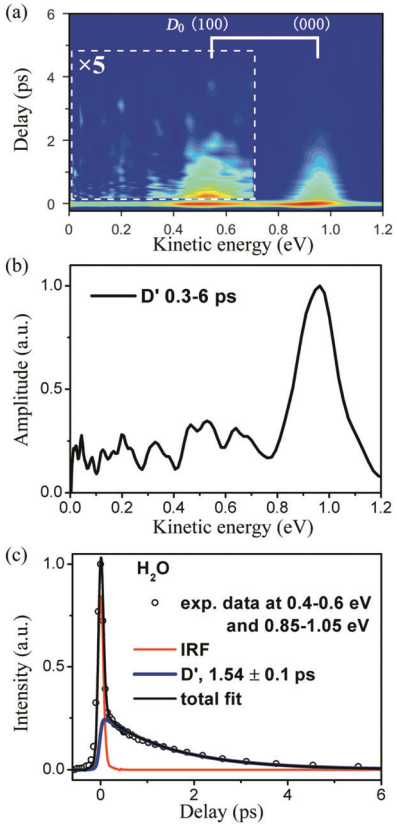

Fig. 2 (a) TRPES of H_2O excited by two-photon absorption at 236.5 nm, after subtracting the background photoelectron generated from single color multiphoton ionization. The kinetic energies of the photoelectron corresponding to ionization to $D_0(000)$ and (100) are indicated by the white comb structure. A portion of the TRPES data is scaled by a factor of 5 for better presentation. (b) The kinetic energy distribution of the photoelectron derived by integrating the TRPES in (a) over the time delay range of 0.3–6 ps. (c) The experimental photoelectron transient derived by integrating the TRPES in (a) over the kinetic energy range of 0.4–0.6 eV and 0.85–1.05 eV. The contributions for each component derived from the least-squares fit are also included. See the text for further details.

0.3–0.5 eV, is shown. Only a time-delay range of 2.73–100 ps is provided where the strong signal around time-zero is negligible. This photoelectron transient is fitted with a single-exponential decay function and a lifetime of 22.6 ± 1.6 ps is derived. The error bars stand for one standard deviation from the fit.

In a high resolution 3 + 1 REMPI spectroscopy study by Ashfold and coworkers, the linewidths of the rotational lines of the origin bands of the $\tilde{D}^1B_1 \leftarrow \tilde{X}^1A_1$ transition were measured.[12] From the linewidths, the lifetimes of the D̃′ state could be estimated: the lifetime of the D̃′(000) vibronic state of H_2O was determined to be around 1.3 ps, showing no rotational state dependence. As for D_2O, the linewidths showed a rotational state dependence as:

$$\omega = 0.05 + 0.01 \times \langle \hat{J}_a^2 \rangle \ \mathrm{cm}^{-1}. \qquad (2)$$

According to this quantitative relationship, the lifetime of the $J = 0$ rotational state is 106 ps, and it quickly decreases with the increase of the $\langle \hat{J}_a^2 \rangle$. The lifetime of H_2O D̃′(000) derived in

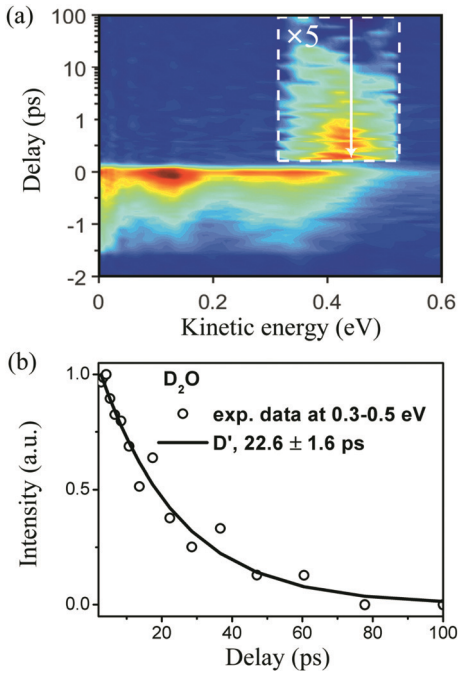

Fig. 3 (a) TRPES of D_2O excited by two-photon absorption at 236.3 nm, after subtracting the background photoelectron generated from single color multiphoton ionization. The energetic limit for ionization to D_0 is indicated by the white arrow. Note that a combination of linear and logarithmic scales is used in the ordinate. A portion of the TRPES data is scaled by a factor of 5 for better presentation. (b) The transient of the photoelectron of 0.3–0.5 eV over the time-delay range of 2.73–100 ps. The curve derived from a single-exponential fit to the experimental transient is also included.

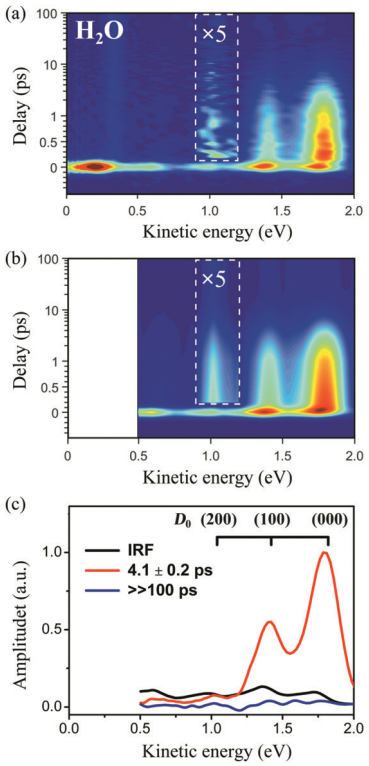

Fig. 4 (a) TRPES of H_2O excited by two-photon absorption at 231.8 nm, after subtracting the background photoelectron generated from single color multiphoton ionization. The TRPES and decay associated spectra derived from a 2D global least-squares fit (see text) are shown in (b) and (c), respectively. The kinetic energies of the photoelectron corresponding to ionization to D_0(000), (100) and (200) are indicated by the black comb structure. Note that a combination of linear and logarithmic scales is used in the ordinate in (a) and (b). A portion of the TRPES data is scaled by a factor of 5 for better presentation.

the current study is in very good agreement with a previous study. As for D_2O, the derived lifetime of 22.6 ± 1.6 ps simply implies a nonzero, but small average rotational angular momentum of the D_2O molecule in the molecular beam which is typically the case.

The $\tilde{D}''^1A_2$ state

The TRPES data of H_2O at a pump wavelength of 231.8 nm are shown in Fig. 4(a). Similar to that for H_2O $\tilde{D}'$, there are also two features: the strong and broad feature around time-zero and three equally spaced peaks showing a decay dynamics of a few ps. These three peaks match very well in kinetic energy with the photoionization to the D_0(000), (100) and (200) vibronic states of H_2O^+.[12,16,17] There are also some very weak, but discernable signals, especially at 0.3 eV, which shows no clear decay within the time delay range employed here (up to 100 ps). This is presumably from the photoionization of some long-lived reaction intermediates or products, such as the H atom product, as found in the study of the ultrafast decay dynamics of the $\tilde{F}$ states.[8]

A 2D global least-squares method was employed to simultaneously fit data at all time delay and a kinetic energy range of 0.5–2.0 eV. The photoelectron at lower kinetic energies was not included to avoid interference from the long-lived components. The kinetic model used to fit the TRPES data includes the IRF accounting for the strong feature around time-zero, an exponential decay function for the three peaks and a component with a lifetime much longer than 100 ps accounting for the long-lived components. The TRPES data derived from the fit and the decay associated spectra for each component are shown in Fig. 4(b) and (c). The fitting quality is satisfactory and a lifetime of 4.1 ± 0.2 ps is derived for the H_2O $\tilde{D}''$(000). In the fit, the time-zero and IRF were varied in their own ranges to obtain the best fit. The confidence interval of the time constant was estimated by considering two potential reasons: (1) the uncertainty of the time constant was estimated by varying the time-zero and IRF in their own range; (2) one standard deviation from the fit itself. The error bar given here stands for a combination of both sources.

The overall profile of the TRPES data for D_2O $\tilde{D}''$ (Fig. 5(a)) is very similar to that of the TRPES data for H_2O $\tilde{D}''$. However, the 2D global fit to it turned out to be much more complicated and revealed that the time decay dependence of three peaks is not single-exponential and the weakest peak at the lowest kinetic energy shows a delayed rise followed by a decay, suggesting the presence of a sequential process. As such, data analysis was done in another way which included two steps: (1) the photoelectron transient of the two peaks at higher kinetic energies

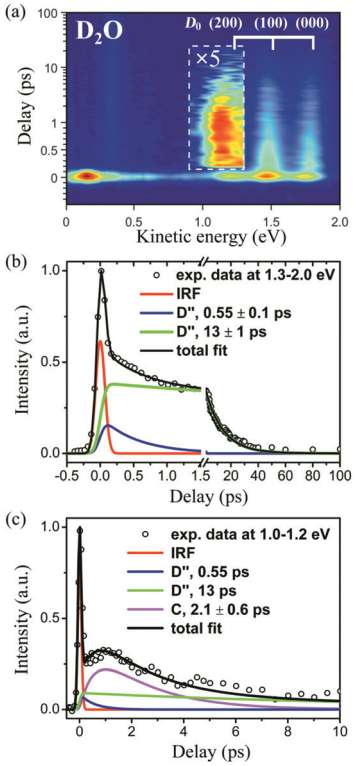

Fig. 5 (a) TRPES of D_2O excited by two-photon absorption at 232.0 nm, after subtracting the background photoelectron generated from single color multiphoton ionization. The kinetic energies of the photoelectron corresponding to ionization to D_0(000), (100) and (200) are indicated by the white comb structure. Note that a combination of linear and logarithmic scales is used in the ordinate. A portion of the TRPES data is scaled by a factor of 5 for better presentation. (b) The experimental photoelectron transient derived by integrating the TRPES in (a) over the kinetic energy range of 1.3–2.0 eV. The contributions for each component derived from the least-squares fit are also included. (c) Same as (b), but for the photoelectron range over 1.0–1.2 eV.

was fit first. It was well fitted with a model including two exponential decay functions, and the IRF accounting for the extremely fast decaying feature around time-zero (Fig. 5(b)). It was also found that the two exponentially decaying components have a parallel relationship, *i.e.*, either these two components are excited simultaneously and decay independently, or they are from the same excited-state wavepacket which decays by two independently pathways at their own rate. The two time constants were derived to be 0.55 ± 0.1 and 13 ± 1 ps, respectively. (2) In the second step, the photoelectron transient for the peak with the lowest kinetic energy was analyzed. For this transient, two components derived in the first step are expected to present, as suggested by the analysis of the TRPES data of H_2O $\tilde{D}'$. A model including three exponential decay functions and the IRF was used. Two of three time constants were fixed to 0.55 and 13 ps, in order to reduce the number of the free varying parameters and make the fit converging easier. The fit quality was reasonable (Fig. 5(c)). The other time constant is derived to be 2.1 ± 0.6 ps. The fitting procedure showed a scenario as follows: at time-zero, there are two components which decay independently with time constants of 0.55 ± 0.1 and 13 ± 1 ps, respectively. The former is followed by the third component which itself decays with a time constant of 2.1 ± 0.6 ps. This sequential process corresponds to the delayed rise in the photoelectron transient. The error bars for these time constants were estimated in a similar way as that for the $\tilde{D}'$ state of H_2O.

D_2O is excited to the $\tilde{D}''$(000) state which decays through two independent pathways with 0.55 ± 0.1 and 13 ± 1 ps time constants. The former pathway is to a lower electronic state which itself decays with a lifetime of 2.1 ± 0.6 ps. This lower electronic state is assigned to the $\tilde{C}^1B_1$ state for the following reasons: (1) the $\tilde{C}$ state is a Rydberg state with an electron from the highest occupied molecular orbital (HOMO) excited to the $3pa_1$ Rydberg orbital and it possesses a minimum energy geometry very close to that of D_2O^+ D_0, resulting in the photoionization process being dominated by diagonal Franck–Condon (FC) factors ($\Delta\nu = 0$) and the vibrational energy of the neutral D_2O being retained in the cation upon ionization. As such, the kinetic energy of the emitted electron can be readily calculated using the adiabatic excitation energy of the $\tilde{C}$ state,[18,19] the adiabatic ionization potential[15] and the probe photon energy. At the probe wavelength used here (330.8 nm), the photoelectron kinetic energy is expected to be 1.1 eV, in very good agreement with the experimentally measured TRPES data. The photoelectron associated with photoionization of D_2O $\tilde{D}''$(000) to D_2O^+ D_0(200) is expected to have a kinetic energy of ~1.2 eV, making itself unresolved from the contribution of the $\tilde{C}$ state, as shown in Fig. 5(a). (2) In a previous study, the lifetime of the $\tilde{C}$ state was measured and the (000), (010) and (100) vibrational states are of 5.76, 4.0 and 3.6 ps, respectively, showing a gradual decrease of lifetime with the increase of the vibrational energy.[6] The vibrational energy of the $\tilde{C}$ state following the decay of the D″ state is expected to be close to that of $\tilde{C}$(130) and the lifetime of 2.1 ± 0.6 ps is in line with the vibrational energy dependence of the $\tilde{C}$ state lifetime.

There are two time constants, 0.55 ± 0.1 and 13 ± 1 ps, for D_2O $\tilde{D}''$. The latter shows a "normal" H ↔ D isotopic substitution effect (τ_{D_2O}/τ_{H_2O}) of ~3.2, while the former an "abnormal" isotopic substitution effect of ~1/7. The decay pathway of D_2O $\tilde{D}''$ with 13 ± 1 ps time constant is most likely the same as that for H_2O $\tilde{D}''$. The $\tilde{D}'' \rightarrow \tilde{C}$ pathway is hitherto unobserved and only presents for D_2O. The nonadiabatic coupling between the $\tilde{D}''$ and $\tilde{C}$ states might be through two different mechanisms: vibronic coupling or Coriolis interaction. The vibrational states of the $\tilde{C}$ electronic state hold a symmetry of A_2 or B_1 for the odd or even quanta of the ν_3 mode, respectively. The $\tilde{D}''^1A_2$(000) state can be coupled to the $\tilde{C}$ vibronic state of the A_2 symmetry only through vibronic interaction, while those of the B_1 symmetry only through Coriolis interaction induced by the rotation around the *c*-axis of the molecule. The $\tilde{D}''$ state is about 5500 cm^{-1} higher than the $\tilde{C}$ state and, therefore, it would be very surprising if the vibronic coupling between the $\tilde{D}''$ and $\tilde{C}$ states only plays a role in D_2O.[12,17–19] Therefore, we suggest that the $\tilde{D}'' \rightarrow \tilde{C}$ decay pathway is induced *via* Coriolis interaction. This also provides one of the possible reasons of the two independent decay pathways for D_2O: the rotational state of zero or very small $\hat{J}_c$ decays to some lower electronic states with a time constant of

13 ± 1 ps, while those of higher $\hat{J}_c$ decays to the $\tilde{C}$ state through Coriolis interaction with a time constant of 0.55 ± 0.1 ps. The fact that the decay pathway of $\tilde{D}'' \rightarrow \tilde{C}$ is only observed for D_2O implies that there might be some near resonance between $\tilde{D}''(000)$ and one or more vibrational states of the $\tilde{C}$ state, greatly enhancing the role that the Coriolis interaction plays. As for H_2O, such near resonance is absent and the $\tilde{D}'' \rightarrow \tilde{C}$ decay pathway is not discernable. The larger rotational constants of H_2O due to the smaller mass of the H atom relative to the D atom make the attainable $\hat{J}_c$ of the H_2O molecule in the molecular beam smaller, further limiting the role of $\tilde{D}'' \rightarrow \tilde{C}$ pathway in the decay of H_2O $\tilde{D}'(000)$.

In summary, D_2O $\tilde{D}''(000)$ decays through two independent pathways depending on the rotation around the *c*-axis of the molecule: those with zero and very small $\hat{J}_c$ decay with a time constant of 13 ± 1 ps, and those with a higher $\hat{J}_c$ decay to the $\tilde{C}$ state *via* Coriolis interaction with a much smaller time constant of 0.55 ± 0.1 ps. As for H_2O $\tilde{D}''(000)$, only the former decay pathway is observed, with a time constant of 4.1 ± 0.2 ps.

Conclusions

The ultrafast decay dynamics of water molecules excited to $\tilde{D}'^1B_1$ and $\tilde{D}''^1A_2$ states is studied by combining two-photon excitation and time-resolved photoelectron imaging techniques. The lifetime of the $\tilde{D}'^1B_1(000)$ state of H_2O (D_2O) is determined to be 1.54 ± 0.1 (22.6 ± 1.6) ps, consistent with a previous high-resolution spectroscopic study by Ashfold and coworkers. The H_2O $\tilde{D}''^1A_2(000)$ state decays with a lifetime of 4.1 ± 0.2 ps, while for the D_2O $\tilde{D}''^1A_2(000)$ state, two independent decay pathways are observed, with time constants of 0.55 ± 0.1 and 13 ± 1 ps. The former is proposed to be associated with a hitherto undocumented $\tilde{D}'' \rightarrow \tilde{C}$ pathway, *via* Coriolis interaction induced by rotation around the molecular *c*-axis. The pathway associated with the latter time constant is presumably the same as that for H_2O $\tilde{D}''^1A_2(000)$.

Conflicts of interest

There are no conflicts to declare.

Acknowledgements

This work was supported by the National Natural Science Foundation of China (Grant No. 21833003 and 21573228) and the Strategic Priority Research Program of the Chinese Academy of Sciences (No. XDB17000000).

References

1 S. Bell, *J. Mol. Spectrosc.*, 1965, **16**, 205.
2 M. N. R. Ashfold, J. M. Bayley and R. N. Dixon, *Chem. Phys.*, 1984, **84**, 35.
3 A. Hodgson, J. P. Simons, M. N. R. Ashfold, J. M. Bayley and R. N. Dixon, *Mol. Phys.*, 1985, **54**, 351.
4 O. Steinkellner, F. Noack, H.-H. Ritze, W. Radloff and I. V. Hertel, *J. Chem. Phys.*, 2004, **121**, 1765.
5 K. Yuan, R. N. Dixon and X. Yang, *Acc. Chem. Res.*, 2011, **44**, 369.
6 Z. G. He, D. Y. Yang, Z. C. Chen, K. J. Yuan, D. X. Dai, G. R. Wu and X. M. Yang, *Phys. Chem. Chem. Phys.*, 2017, **19**, 29795.
7 X. Hu, L. Zhou and D. Xie, *WIREs Comput. Mol. Sci.*, 2018, **8**, 1350.
8 D. Y. Yang, Y. J. Min, Z. Chen, G. Z. He, Z. C. Chen, K. J. Yuan, D. X. Dai, G. R. Wu and X. M. Yang, *Chin. J. Chem. Phys.*, 2019, **32**, 59.
9 K. Yuan, Y. Cheng, L. Cheng, Q. Guo, D. Dai, X. Wang, X. Yang and R. N. Dixon, *Proc. Natl. Acad. Sci. U. S. A.*, 2008, **105**, 19148.
10 K. J. Yuan, Y. A. Cheng, L. N. Cheng, Q. Guo, D. X. Dai, X. M. Yang and R. N. Dixon, *J. Chem. Phys.*, 2010, **133**, 134301.
11 H. Wang, Y. Yu, Y. Chang, S. Su, S. Yu, Q. Li, K. Tao, H. Ding, J. Yang, G. Wang, L. Che, Z. He, Z. Chen, X. Wang, W. Zhang, D. Dai, G. Wu, K. Yuan and X. Yang, *J. Chem. Phys.*, 2018, **148**, 124301.
12 M. N. R. Ashfold, J. M. Bayley and R. N. Dixon, *Can. J. Phys.*, 1984, **62**, 1806.
13 Z. G. He, Z. C. Chen, D. Y. Yan, D. X. Dai, G. R. Wu and X. M. Yang, *Chin. J. Chem. Phys.*, 2017, **30**, 247.
14 G. A. Garcia, L. Nahon and I. Powis, *Rev. Sci. Instrum.*, 2004, **75**, 4989.
15 U. Jacovella and F. Merkt, *Mol. Phys.*, 2015, **113**, 3918.
16 S. Y. Truong, A. J. Yencha, A. M. Juarez, S. J. Cavanagh, P. Bolognesi and G. C. King, *Chem. Phys.*, 2009, **355**, 183.
17 R. D. Gilbert, M. S. Child and J. W. C. Johns, *Mol. Phys.*, 1991, **74**, 473.
18 J. W. C. Johns, *Can. J. Phys.*, 1963, **41**, 209.
19 P. Gurtler, V. Saile and E. E. Koch, *Chem. Phys. Lett.*, 1977, **51**, 386.